ACS APPLIED NANO MATERIALS

www.acsanm.org

Article

Hybrid $Ti_3C_2T_x$ MXene and Carbon Nanotube Reinforced Epoxy Nanocomposites for Self-Sensing and Structural Health Monitoring

Ming Dong,* Oliver Tomes, Aaron Soul, Yi Hu, Emiliano Bilotti, Han Zhang, and Dimitrios G. Papageorgiou*

Cite This: *ACS Appl. Nano Mater.* 2024, 7, 3314−3325

Read Online

ACCESS | Metrics & More | Article Recommendations | Supporting Information

ABSTRACT: Herein we present the transformative effects of multiwall carbon nanotube (MWCNT)-MXene hybrid nanofillers on the mechanical, electrical, and piezoresistive properties of the resulting epoxy nanocomposites. The utilization of the MWCNT-MXene hybrids significantly improves the dispersion of fillers within the epoxy matrix, effectively eliminating the agglomeration of individual fillers and improving the stress transfer efficiency. With just 1 wt % MWCNT-MXene hybrid, we observed improvements in the Young's modulus and the flexural modulus, which increased by 31 and 28%, respectively, when compared to neat epoxy. Furthermore, the fracture toughness of these composites was 84.5% higher than that of neat epoxy, primarily attributed to crack deflection and filler debonding mechanisms. The hybrid composites exhibited increased piezoresistive sensitivity during tensile, flexural, and fracture tests due to the creation of a percolating network of MWCNT and MXene nanoplatelets. Our findings have implications for the development of advanced hybrid materials, holding promise for applications in strain sensors and self-sensing structures.

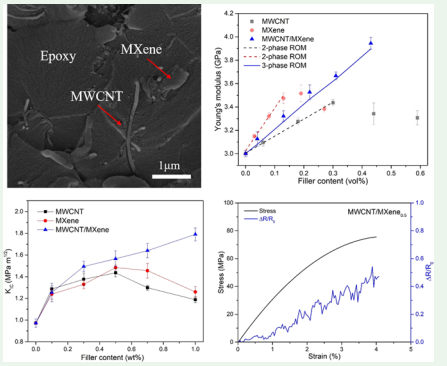

KEYWORDS: *MXene ($Ti_3C_2T_x$), MWCNT, epoxy, nanocomposites, mechanical, electrical*

1. INTRODUCTION

Over the last few decades, thermosets have gained widespread utilization as essential structural and engineering materials, thanks to their exceptional mechanical and physical attributes. Among thermoset materials, epoxy resins stand out as a significant representative, renowned for their important features that include minimal shrinkage during the curing process, high tensile strength, and remarkable resistance to chemicals and heat.[1] Consequently, epoxy resins have found extensive applications in a variety of industries, including but not limited to coatings, adhesives, electronics, and aerospace.[2] Nevertheless, epoxy resins do come with inherent drawbacks, notably their limited fracture toughness and low electrical conductivity, which have constrained their utilization across multiple domains.

The incorporation of nanofillers into epoxy resins stands as an effective strategy for improving not only their mechanical performance but also endow them with multifunctional properties.[3−5] Among different nanofillers, carbon-based nanomaterials such as carbon nanotubes (CNTs) and graphene-related materials have attracted significant interest for their role in enhancing the strength, electrical conductivity, and multifunctionality of epoxy resins.[6,7] CNTs, possessing a one-dimensional (1D) structure, showcase remarkable attributes, including a high elastic modulus, superb conductivity, and high aspect ratio.[8,9] Effective reinforcement can be attained when CNTs are evenly dispersed within the matrix, preventing any form of agglomeration.[10] A low electrical percolation threshold in CNT-epoxy composites has been achieved thanks to their unique structure and high conductivity.[11] Compared to CNTs, graphene nanoplatelets (GNPs), a layered two-dimensional (2D) carbon allotrope, offer distinct advantages in enhancing the mechanical properties of polymer composites. This advantage arises from their planar structure and high specific surface area, which enable superior stress transfer efficiency from the matrix to the filler during loading.[12,13] Both of these characteristics play an important role in reinforcing epoxy composites.

MXenes, known as transition metal carbide and nitrides, have attracted significant research attention since the synthesis of $Ti_3C_2T_x$ in 2011.[14] From a morphological perspective, MXenes share similarities with graphene, appearing as stacked sheets. Notably, $Ti_3C_2T_x$ MXene displays an elastic modulus of approximately 330 GPa[15] and exceptional electrical conductivity reaching up to 11,000 S cm^{-1}.[16] These properties make MXenes an appealing choice for improving mechanical,[17] optical,[18] and electromagnetic interference shielding[19,20]

Received: November 30, 2023
Revised: January 3, 2024
Accepted: January 8, 2024
Published: January 23, 2024

Scheme 1. Dispersion of $Ti_3C_2T_x$ MXene and MWCNT in the Epoxy Matrix by a Three-Roll Milling Process

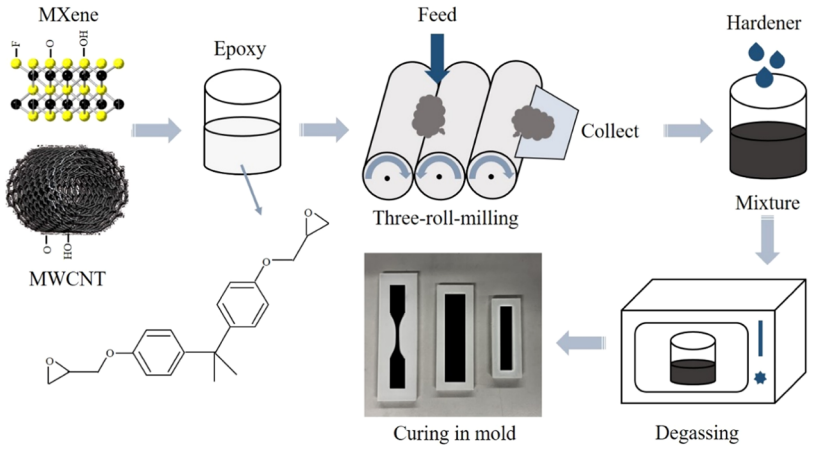

properties of polymer nanocomposites. Recently, studies on the properties of MXene-incorporated epoxy nanocomposites started to receive attention.[21,22] It has been shown that the incorporation of MXene nanoplatelets can improve mechanical properties,[23,24] thermal conductivity,[25,26] and electrical conductivity[22,27] of epoxy nanocomposites. For example, the thermal conductivity of epoxy resin was improved by 141.3% to 0.587 W/mk with 1.0 wt % Ti_3C_2 MXene filler.[28] In another study, the electrical conductivity of epoxy resin was improved to 4.52×10^{-4} S/m with 1.2 wt % $Ti_3C_2T_x$ MXene.[27] These findings underscore the potential of MXenes in enhancing the performance of epoxy nanocomposites.

Nevertheless, the tendency of MXenes to restack and agglomerate even at low filler concentrations has constrained their reinforcing effectiveness in epoxy nanocomposites.[21] In contrast, several hybrid nanofillers have demonstrated greater efficacy in enhancing the mechanical and functional properties of polymer nanocomposites compared to individual fillers, primarily owing to synergistic effects,[29−31] which are closely related to the hybrid filler structure, the interfacial interactions between hybrids, and the improvements in dispersion of both components.[32] Among the list of hybrids, CNTs have been widely combined with GNP or graphene oxide (GO) to improve mechanical, thermal, and electrical properties of epoxy nanocomposites synergistically.[33−36] It has been illustrated that the stacking of 2D GNP or GO and the aggregation of 1D CNT have been effectively constrained by fabricating a complex three-dimensional (3D) structure within the hybrid nanocomposites. On that basis, CNTs have been combined with MXenes to fabricate polymer nanocomposites that display synergistic effects.[37−39]

To the best of our knowledge, no studies have explored the combination of MXene nanoplatelets and CNTs for reinforcing epoxy nanocomposites. This work addresses this literature gap by effectively dispersing multiwall carbon nanotube (MWCNT) and MXene into epoxy resin using a three-roll mill. The morphology of the fillers was characterized by X-ray diffraction (XRD), Raman spectroscopy, and scanning electron microscopy (SEM). Finally, the mechanical, electrical, and piezoresistive properties of the fabricated epoxy nanocomposites were investigated in detail.

2. EXPERIMENTAL SECTION

2.1. Materials. The Ti_3AlC_2 MAX powder with a particle size of 38 μm was purchased from Jilin 11 Technology Co., Ltd. Lithium fluoride (LiF, 98.5% grade) powder and hydrochloric acid (HCl, ACS reagent) were provided by Sigma-Aldrich. IB2 Epoxy Bio Resin and IB2 Epoxy Hardener were obtained from Easy Composites. Multiwalled carbon nanotubes (MWCNTs) with an inner diameter of 3−5 nm, an outer diameter of 8−15 nm, and a length of 3−12 μm were purchased from Shenzhen Liguangrun E-commerce Co., Ltd. All of the materials were used as received without purification.

2.2. Synthesis of $Ti_3C_2T_x$ MXene. $Ti_3C_2T_x$ MXene was prepared by the in situ HF etching method.[40] First, 1.6 g of LiF was added into 20 mL of 9 M HCl under magnetic stirring at room temperature. Then, 1 g of Ti_3AlC_2 powder was gradually added to the solution with over the course of 5 min to avoid overheating of the reaction. After that, the reaction was brought to a water bath of 40 °C and allowed to run under stirring for 40 h. The resulting mixture was washed with DI water and centrifuged at 3500 rpm for 5 min for each cycle until the pH reached neutral. The products were collected and bath sonicated in DI water for 1 h under argon bubbling to minimize oxidation. Then, a colloidal solution of MXene was collected by centrifugation at 3500 rpm for 1 h. Finally, $Ti_3C_2T_x$ MXene powder was obtained after freeze-drying for 48 h.

2.3. Preparation of Epoxy/MXene/MWCNT Nanocomposites. In this study, epoxy nanocomposites with $Ti_3C_2T_x$ MXene and MWCNT were fabricated using a three-roll mill[41,42] as shown in Scheme 1. A certain amount of MXene, MWCNT, or the hybrid powders were dispersed in the epoxy resin at 70 °C for 10 min under magnetic stirring. The weight ratio of MWCNT to MXene was 1:1 in the hybrid (0.1, 0.3, 0.5, 0.7, and 1 wt %).[43] Then, the mixtures were fed into a three-roll miller (80E EXAKT GmbH, Germany). The gap between the feed roll and the apron roll reduced gradually (90:30, 60:20, 45:15, 30:10, and 15:5 μm) as previously reported.[44] The speed of the roller was fixed at 200 rpm, and the mixtures passed through each gap distance for two cycles.

To prepare epoxy nanocomposites, the hardener was added in a 22:100 weight ratio to the epoxy. The mixture was manually mixed for 5 min, which was then degassed under vacuum for 40 min. The pure epoxy and epoxy nanocomposites were prepared by curing the mixture at room temperature for 16 h and then at 40 °C for 24 h as suggested by the supplier, which should lead to optimal mechanical properties of the epoxy resin.

2.4. Characterization. X-ray diffraction (XRD) of the samples were recorded on an ANalytical X'Pert-Pro diffractometer using standard short set (reflection mode, Cu Kα radiation, divergence slit, and Ni-filter). The scanning scope of 2θ was 5−70° at room temperature. Raman spectroscopy was performed by using a Renishaw inVia Raman microprobe system. A laser excitation of 785 nm with a grating of 1200 grooves/mm was used. The laser power was kept below 1 mW to avoid the laser heating effects. Morphological studies were carried out using scanning electron microscopy (SEM, FEI Inspect-F, Netherlands) with an acceleration voltage of 5 kV. $Ti_3C_2T_x$ MXene and MWCNT samples were

https://doi.org/10.1021/acsanm.3c05728
ACS Appl. Nano Mater. 2024, 7, 3314−3325

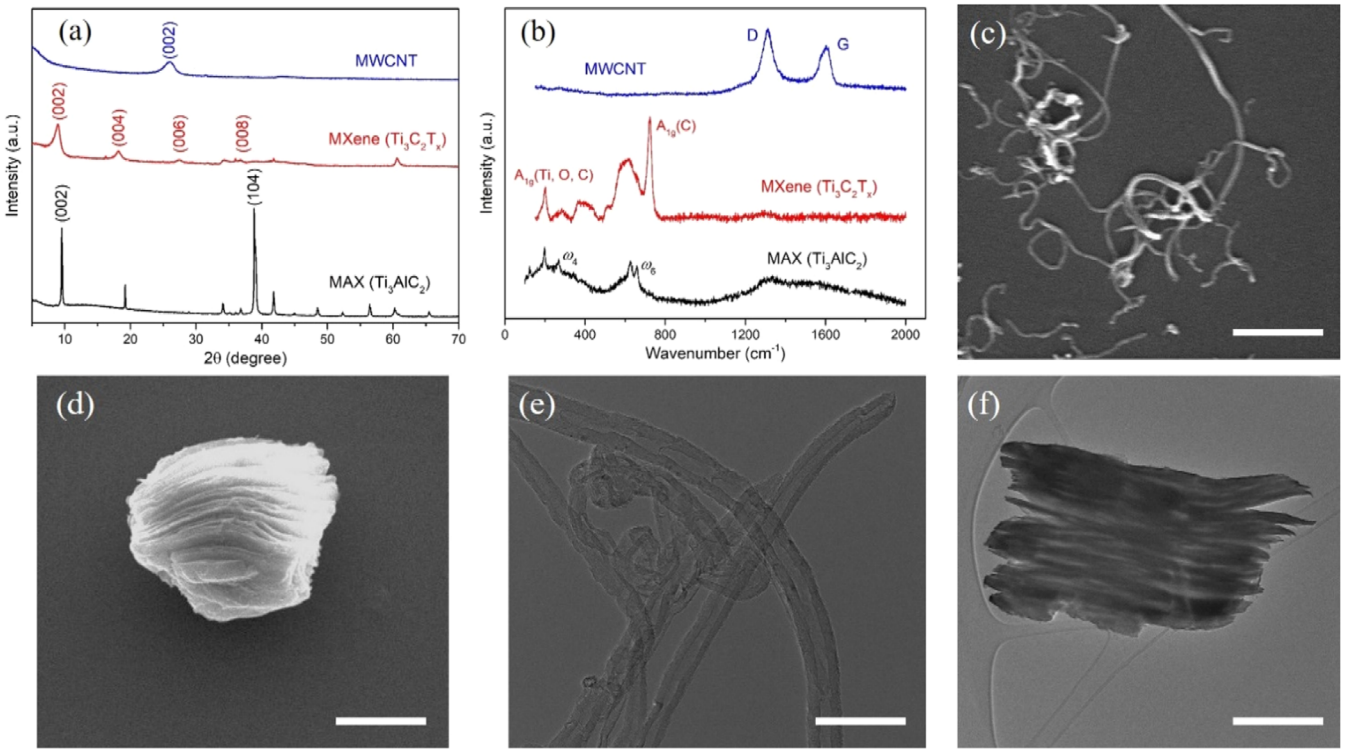

Figure 1. (a) XRD patterns of Ti_3AlC_2 MAX, $Ti_3C_2T_x$ MXene, and MWCNT. (b) Raman spectra of Ti_3AlC_2 MAX, $Ti_3C_2T_x$ MXene, and MWCNT. (c) SEM image of MWCNTs. Scale bar, 500 nm. (d) SEM image of $Ti_3C_2T_x$ MXene with an accordion structure. Scale bar, 2.5 μm. (e) TEM image of MWCNTs. Scale bar, 50 nm. (f) TEM image of $Ti_3C_2T_x$ MXene. Scale bar, 1 μm.

deposited onto a silicon wafer. Fracture surfaces of the cured epoxy composites were obtained by fracture in liquid nitrogen. High-resolution transmission electron microscopy (TEM) imaging was conducted by using a JEOL F200 instrument. Fourier transform infrared spectroscopy (FTIR) tests were performed by using a Smart iTX Optical Base and an AR Diamond Crystal Plate for the Nicolet iS 10.

The tensile, flexural, and fracture properties of pure epoxy and epoxy nanocomposites were characterized by using Instron 5967−1. For the tensile tests, the samples were fabricated according to ASTM D638 TYPE V. A loading cell of 1 kN and a loading rate of 1 mm/min were used. The applied strain was measured by a noncontact video extensometer. For bending tests, the rectangular samples with 56 mm length, 13 mm width, and 1.5 mm thickness were fabricated. The support span was 34 mm, and the crosshead speed was 10 mm/min. For fracture toughness, the single-edge-notched bend (SENB) test was conducted, and rectangular specimens with 40 mm (length) × 4 mm (width) and 8 mm (thickness) were fabricated. The distance between the supporting rollers of the three-point bending test was 32 mm, and the crosshead speed was 10 mm/min. For each specimen, a notch 4 mm deep was machined, and a natural crack was made by tapping a razor blade into the notch. The fracture toughness, K_{IC}, was calculated using the following equation[45]

$$K_{IC} = \frac{FL}{Bw^{3/2}} f(x) \quad (1)$$

$$f(x) = 3x^{1/2}\left\{\frac{[1.99 - x(1-x)(2.15 - 3.93x + 2.7x^2)]}{2(1+2x)(1-x)^{3/2}}\right\} \quad (2)$$

where $x = a/w$, a is the crack length, w, L, and B are the width, length, and thickness of the specimen, and F is the maximum force.

The electrical conductivity of the samples was measured by using a two-probe method using a picoammeter (Keithley 6485, Textronix) and a DC voltage source (Agilet 6614C). The dimensions of the specimens were 56 × 13 × 1.5 mm^3. Silver paste was applied to both ends of the specimens to reduce the contact resistance. A voltage of 10 V was used.

The strain sensing behavior of the nanocomposites was characterized by using the two-probe method where the variation in electrical resistance was monitored with the applied strain or displacement. After the outer epoxy layer was removed, the electrodes were attached to the surfaces of the nanocomposites. For the tensile samples, the distance between the two electrodes was 10 mm. For flexural and fracture tests, two electrodes were directly applied to the two ends of the specimen. Constant voltage of 10 V was applied throughout the experiment.

3. RESULTS AND DISCUSSION

3.1. Morphology of MXene and MWCNT. The $Ti_3C_2T_x$ MXene was produced using the in situ HF etching method, involving the removal of the Al layer from the Ti_3AlC_2 MAX phase by employing a mixture of LiF and HCl. Figure 1a presents the XRD analysis illustrating the structural transformation from the Ti_3AlC_2 MAX phase to $Ti_3C_2T_x$ MXene. In the case of Ti_3AlC_2 MAX, the distinctive peak at 2θ = 38.8° (104) is indicative of the presence of Al. This specific peak was absent in the XRD spectra of the synthesized $Ti_3C_2T_x$ MXene, confirming the successful etching of the Al layers through the in situ HF process.[46] Furthermore, the characteristic (002) peak at 2θ = 9.5° experienced a shift toward a lower value at 2θ = 8.9° and displayed broadening, indicating an increase in d-spacing. Additionally, three new peaks corresponding to the (004), (006), and (008) crystal planes emerged in the XRD pattern of $Ti_3C_2T_x$.[40] The XRD pattern of the MWCNT is also presented in Figure 1a. The sharpness of the (002) peak in the MWCNT indicates the presence of a well-defined graphite structure.

Figure 1b shows the Raman spectra of Ti_3AlC_2 MAX, $Ti_3C_2T_x$ MXene, and MWCNT in the range of 150−2000

https://doi.org/10.1021/acsanm.3c05728
ACS Appl. Nano Mater. 2024, 7, 3314−3325

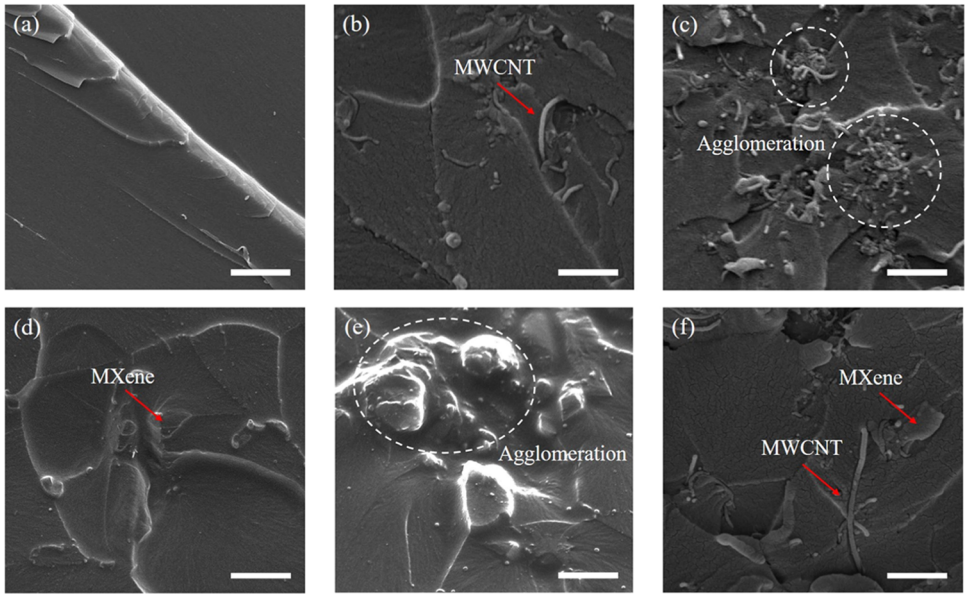

Figure 2. SEM images of fractured surface of (a) neat epoxy and epoxy nanocomposites with (b) 0.5 wt % MWCNT, (c) 1 wt % MWCNT, (d) 0.5 wt % $Ti_3C_2T_x$ MXene, (e) 1 wt % $Ti_3C_2T_x$ MXene, and (f) 1 wt % MWCNT/$Ti_3C_2T_x$ MXene hybrid. Scale bars, 1 μm.

cm^{-1}. For MWCNT, two characteristic peaks, one of the D band at 1310 cm^{-1} and one of the G band at 1598 cm^{-1}, were observed. The D band represents the structural defects and the G band represents the in-plane vibration of the sp^2 bonds.[47] The intensity ratio of the D band to the G band was calculated to be about 1.7, which means that there is a certain degree of defects on the carbon nanotubes. These defects can be ascribed to bonding irregularities in sp^3 configuration, as well as kinks and twists in the structure of MWCNT.[48] For Ti_3AlC_2 MAX and $Ti_3C_2T_x$ MXene, all of the Raman bands were located between 150 and 800 cm^{-1}. The out-of-plane ω_4 peak of Ti_3AlC_2 MAX moved to lower wavenumber for $Ti_3C_2T_x$ MXene (A_{1g} (Ti, O, C)), as Al was etched away and C and surface groups were involved in vibration. In addition, the out-of-plane peak of Ti_3AlC_2 (ω_6) moved to higher wavenumber in the case of $Ti_3C_2T_x$ (A_{1g} (C)).[49] These observations indicate the successful etching of the Al layers.

The SEM micrographs of MWCNT and $Ti_3C_2T_x$ MXene are shown in Figure 1c,1d. It can be seen that MWCNTs show long and tortuous morphologies entangling with each other. The length of MWCNTs ranges from hundreds of nanometers to several micrometers. The SEM image of Ti_3AlC_2 MAX revealing a compact and layered morphology is shown in Figure S1 in the Supporting Information. In contrast, the exfoliated $Ti_3C_2T_x$ MXene exhibits a loose accordion-like structure, which further proves the successful etching and intercalation processes. The TEM images of MWCNT and $Ti_3C_2T_x$ MXene are also shown in Figure 1e,1f. The multiwalled structure of MWCNT with a hollow internal channel and the accordion-like structure of $Ti_3C_2T_x$ MXene were clearly observed.

3.2. Microstructure of Epoxy Nanocomposites. The morphologies of fractured epoxy and epoxy/MXene/MWCNT nanocomposite surfaces were investigated by SEM as shown in Figure 2. The fractured surface of neat epoxy was relatively smooth and continuous (Figure 2a). Therefore, the energy required for fracture in neat epoxy is relatively low. Straight ravines and gullies appeared on the fractured cross section, which are common for brittle fractures of pure materials. In contrast, fracture surfaces of epoxy nanocomposites show different morphologies; the roughness of the surfaces increases significantly (Figure 2b–f). For the case of epoxy/MWCNT nanocomposites at low filler contents (Figure 2b), tortuous MWCNTs were randomly and individually distributed in the epoxy matrix. Long entangled MWCNTs lay on the cross section of the epoxy matrix while no aggregates can be seen. The small bright dots on the fractured surface indicate the broken ends of MWCNTs. The pulled out and broken MWCNTs indicate that there is a strong interfacial interaction between MWCNTs and the epoxy, resulting in an effective load transfer from the matrix to the fillers. Therefore, it is expected that the mechanical properties of epoxy nanocomposites with MWCNTs at low loadings could be improved. In contrast, significant agglomeration was observed on the fracture surface of epoxy nanocomposites with 1 wt % MWCNT (Figure 2c). This led to the formation of defects or flaws in the matrix, which acted as stress concentrators and, in turn, restricted the effective stress transfer from the matrix to the filler; as a result, the mechanical properties of the specific nanocomposite samples are expected to be degraded compared to their low-content counterparts.

The flaky shape of MXene nanoplatelets can be seen at the fractured surface of the 0.5 wt % $Ti_3C_2T_x$ MXene nanocomposite sample (Figure 2d). The cracks alter their path and propagate in different planes when encountering the flakes. The fracture area increases and should consume more fracture energy. As a result, the mechanical properties of epoxy nanocomposites are expected to be improved with the incorporation of low MXene loadings. However, further increasing the MXene loading induced agglomeration, as observed in Figure 2e. This induced the formation of cracks, which initiated and propagated easily and, in turn, would reduce the strength of epoxy nanocomposites.

Both MWCNT and MXene can be observed on the fracture surface of epoxy nanocomposites with a 1 wt % MWCNT/$Ti_3C_2T_x$ MXene hybrid (Figure 2f). It can be noticed that better dispersion of MWCNT and MXene was achieved in the MWCNT/MXene hybrid-reinforced nanocomposites. The

https://doi.org/10.1021/acsanm.3c05728
ACS Appl. Nano Mater. 2024, 7, 3314–3325

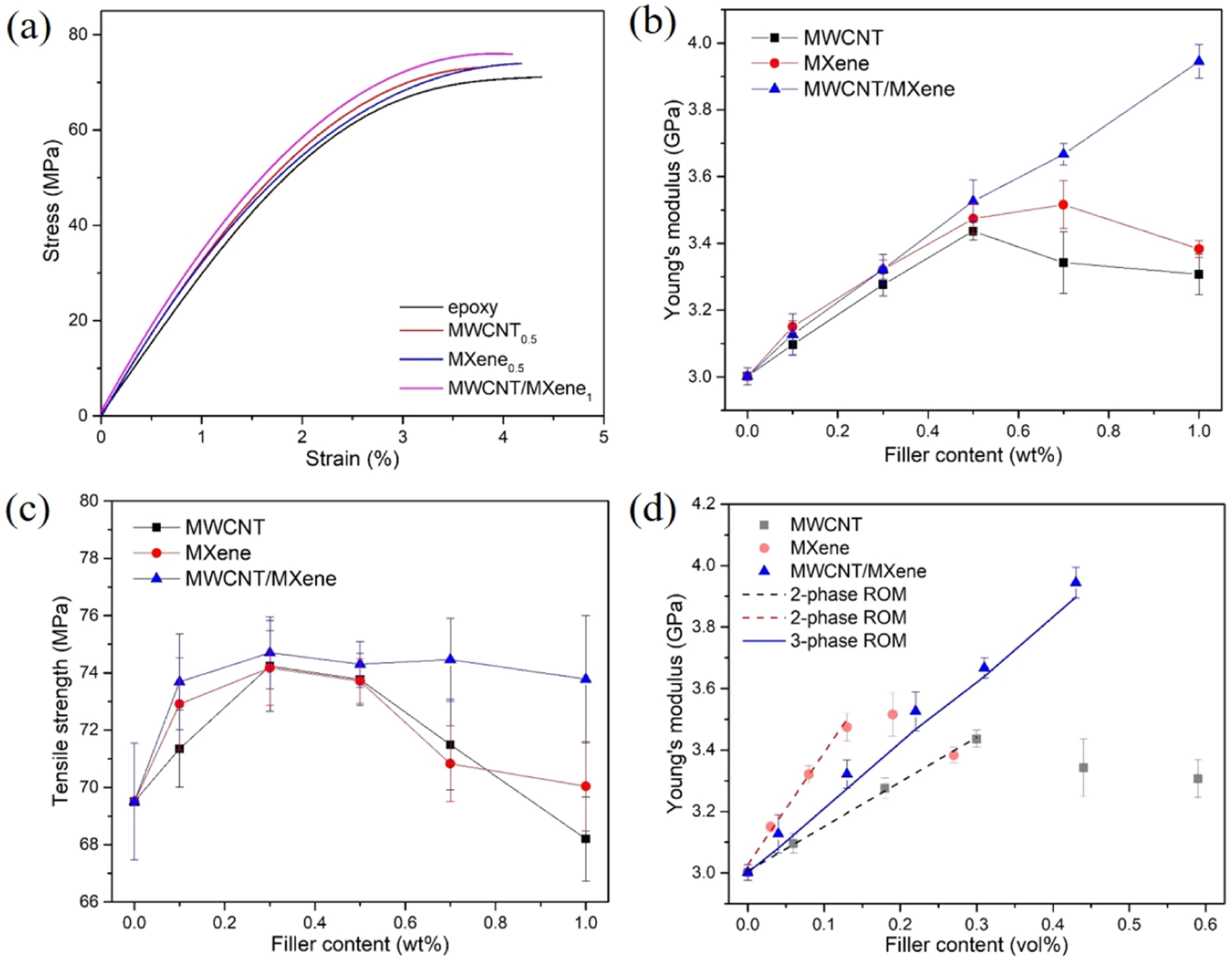

Figure 3. (a) Tensile stress−strain curves of epoxy and epoxy nanocomposites with 0.5 wt % MWCNT, 0.5 wt % MXene, and 1 wt % MWCNT/MXene hybrid. (b) Variation of the Young's modulus of epoxy nanocomposites with MWCNT, MXene, and MWCNT/MXene hybrid. (c) Variation of the tensile strength of epoxy nanocomposites with MWCNT, MXene, and MWCNT/MXene hybrid. (d) Variation of Young's modulus with filler volume content for epoxy nanocomposites with MWCNT, MXene, and MWCNT/MXene hybrid. The results were fitted with the rule of mixtures.

agglomeration that was observed in individual MWCNT and MXene nanocomposites was prevented in this case. This could lead to larger filler/matrix contact area and enhanced interactions between the fillers and the matrix. As a result, the mechanical properties of epoxy nanocomposites with MWCNT/MXene hybrid are expected to be improved.

The interfacial interactions between MWCNT and MXene nanoplatelets were characterized by FTIR as shown in Figure S2a in the Supporting Information. For MWCNT, the spectrum shows bands at 3436 cm^{-1} (assigned to −OH stretching), 2923 and 2854 cm^{-1} (attributed to asymmetric and symmetric CH_2 stretching), 1629 cm^{-1} (assigned to C═C stretching), and 1052 cm^{-1} (attributed to C−O stretching).[50] These functional groups were introduced during the production and purification processes.[50] For MXene, the spectrum shows bands at 3400 cm^{-1} (assigned to −OH stretching), 1623 cm^{-1} (assigned to C−OH bending), and 1056 cm^{-1} (assigned to C−F stretching).[51] For the MWCNT/MXene hybrid, the −OH stretching band moved to 3425 cm^{-1}. This indicates the existence of interfacial interactions between MWCNT and MXene (oxygen-containing groups and hydroxyl groups), which facilitate the dispersion of each filler and promote uniform dispersion of the hybrid filler in the epoxy resin. The underlying mechanism is illustrated in Figure S3 in the Supporting Information. Individual MWCNTs tend to entangle, and MXenes tend to restack at high filler contents. In contrast, the presence of the hybrid filler can prevent entanglement or restacking and promote codispersion of each filler due to the interfacial interactions between the hybrid fillers.

The FTIR spectra of pure epoxy and epoxy composites are shown in Figure S2b in the Supporting Information. The bands assigned to hydroxyl groups of the epoxy resin moved to slightly lower wavenumbers for the composites, which can be attributed to the dipole−dipole interactions or hydrogen bonding between residual polar groups of epoxy and fillers.[36] In addition, the intensity of the C−N bond vibration increased for the composites, indicating the positive effect of the fillers on the epoxy curing regime.[52] The XRD patterns of epoxy and epoxy composites are shown in Figure S4 in the Supporting Information. The distinction between epoxy and epoxy composites is quite difficult due to the very low filler loadings.

https://doi.org/10.1021/acsanm.3c05728
ACS Appl. Nano Mater. 2024, 7, 3314−3325

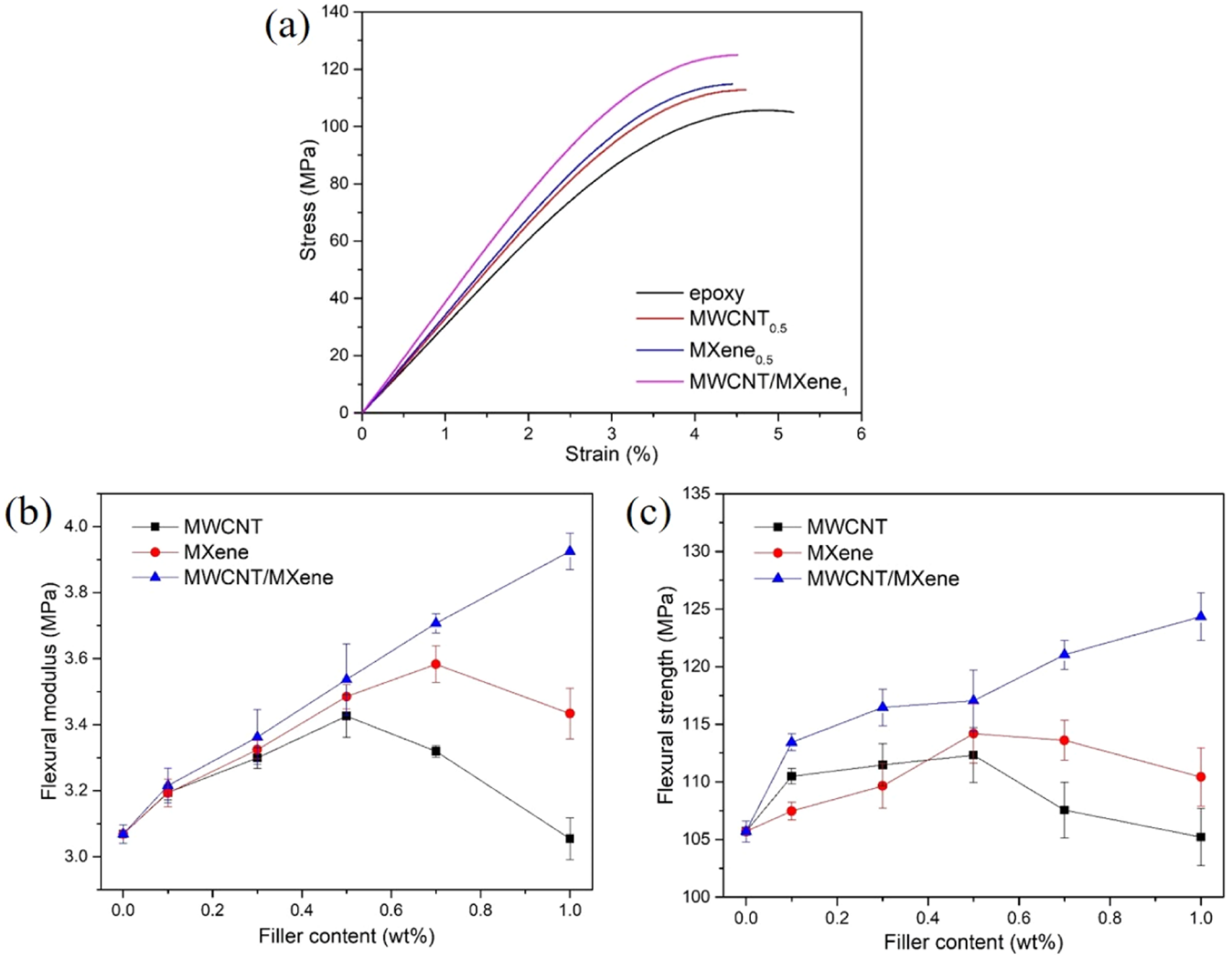

Figure 4. (a) Flexural stress−strain curves of epoxy and epoxy nanocomposites with 0.5 wt % MWCNT, 0.5 wt % MXene, and 1 wt % MWCNT/MXene hybrid. (b) Variation of the flexural modulus of epoxy nanocomposites with MWCNT, MXene, and MWCNT/MXene hybrid. (c) Variation of the flexural strength of epoxy nanocomposites with MWCNT, MXene, and MWCNT/MXene hybrid.

3.3. Mechanical Properties of Epoxy Nanocomposites. *3.3.1. Tensile Properties.* Figure 3a illustrates representative stress−strain curves for neat epoxy and its nanocomposites with 0.5 wt % MWCNT, 0.5 wt % MXene, and 1 wt % MWCNT/MXene hybrid under tensile loading. The nanocomposites exhibit varying degrees of improvement in mechanical properties compared to neat epoxy. In general, both the Young's modulus and tensile strength of epoxy nanocomposites showed enhancements. Notably, individual MWCNTs or MXenes and their hybrids demonstrated similar levels of enhancement at low filler contents, while the hybrids exhibited the highest level of improvement in both Young's modulus and tensile strength at high filler contents (Figure 3b,c). The experimental results for Young's modulus and tensile strength for all nanocomposites are summarized in Figure 3b,3c, respectively. The values are summarized in Table S1 in the Supporting Information. For MWCNT/epoxy and MXene/epoxy nanocomposites, there is an upward trend in the Young's modulus at low filler loading (up to 0.5 wt % for MWCNT and 0.7 wt % for MXene), followed by a declining trend at higher filler loadings. Specifically, the Young's modulus of neat epoxy (3.00 GPa) was improved to 3.44 GPa with 0.5 wt % MWCNT and 3.52 GPa with 0.7 wt % MXene. Conversely, the trend in tensile strength differs from that of Young's modulus. The tensile strength of neat epoxy (69.51 MPa) increased to 73.77, 73.71, and 74.30 MPa, respectively, with the addition of 0.5 wt % MWCNT, MXene, and MWCNT/MXene hybrid. Beyond the 0.5 wt % filler loading, the tensile strength decreased for epoxy/MWCNT and epoxy/MXene nanocomposites, while it remained relatively stable for epoxy/MWCNT/MXene nanocomposites. The improvements in the mechanical properties could be attributed to the uniform dispersion of the fillers at low contents, as shown in Figure 2b,e. Strain can be transferred effectively from the matrix to the fillers at low contents, and higher stress can be sustained due to the intrinsic mechanical properties of MWCNT and MXene nanoplatelets, according to the shear-lag theory.[53] It should be noted that the presence of defects on MWCNTs (as revealed by Raman spectroscopy) would degrade their intrinsic mechanical properties. This is probably one reason why MWCNTs are less effective than MXene nanoplatelets toward reinforcing the Young's modulus of the composites.

The Young's modulus of the composites can be analyzed by the rule of mixtures (ROM).[54,55] Using the two-phase rule of mixtures (ROM) as described in eq s1, we calculated the

https://doi.org/10.1021/acsanm.3c05728
ACS Appl. Nano Mater. 2024, 7, 3314−3325

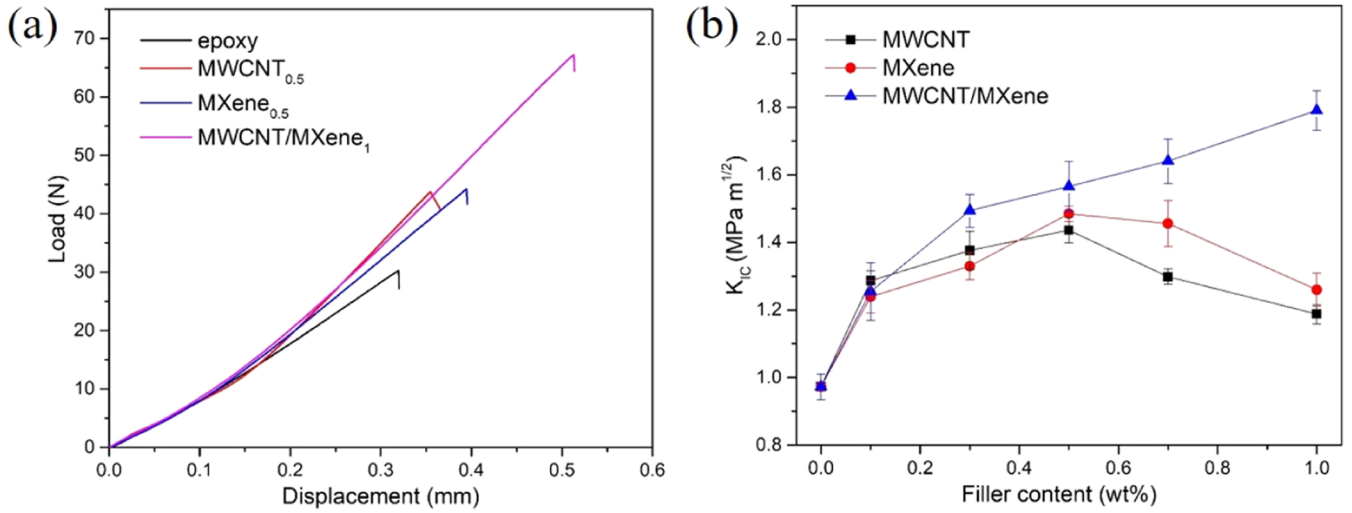

Figure 5. (a) Typical load−displacement curves of epoxy and epoxy nanocomposites with 0.5 wt % MWCNT, 0.5 wt % MXene, and 1 wt % MWCNT/MXene hybrid. (b) Variation of the fracture toughness of epoxy nanocomposites with MWCNT, MXene, and MWCNT/MXene hybrid.

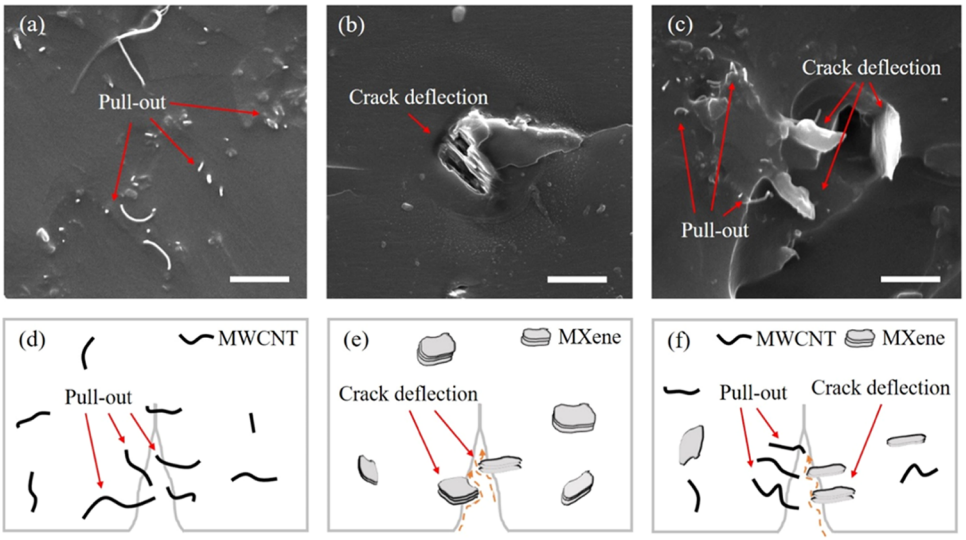

Figure 6. Fracture morphology of epoxy composites with (a) MWCNT (scale bar, 1 μm), (b) MXene (scale bar, 2.5 μm), and (c) MXene/MWCNT (scale bar, 2.5 μm). Schematic illustration of (d) the pull-out of MWCNT, (e) the crack deflection of MXene, and (f) the combination of pull-out and crack deflection.

effective Young's modulus for MWCNT and MXene to be 145.11 and 364.02 GPa, respectively. These relatively high effective modulus values suggest substantial mechanical reinforcement in two-phase nanocomposites at low filler loadings. Subsequently, we applied these calculated modulus values to the three-phase ROM, as outlined in eq s3, and the results for the three-phase system are presented in Figure 3d. It is evident from the figure that the experimental results closely align with the theoretical predictions, indicating the presence of an additive effect between the components of the three-phase system.[55] The limited improvements in the mechanical properties of epoxy nanocomposites beyond the optimum loading can be ascribed to the agglomeration of MWCNTs and MXenes, as shown in Figure 2c,2e, and the difficulties of dispersing the fillers at higher contents. This limitation, in turn, hinders the efficient transfer of stress from the matrix to the fillers, restricting their reinforcing effectiveness. In contrast, the MWCNT/MXene hybrid seems to have facilitated the dispersion of each filler as can be also realized from subsequent SEM images (Figure 2f), allowing for effective stress transfer within the hybrid system.

3.3.2. Flexural Properties. The flexural properties of neat epoxy and its nanocomposites with MWCNT, MXene, and MWCNT/MXene hybrids are shown in Figure 4. Typical flexural stress−strain curves of epoxy and epoxy nanocomposites are illustrated in Figure 4a. Similarly to the tensile properties, the incorporation of MWCNT and MXene into neat epoxy led to improvements in both the flexural modulus and strength. Individual MWCNT and MXene fillers exhibited a similar level of reinforcement, while their hybrid configuration demonstrated the highest level of enhancement. Figure 4b,4c illustrates the changes in the flexural modulus and flexural strength with varying filler loading, respectively. The values are summarized in Table S2 in the Supporting Information. Specifically, the flexural modulus of neat epoxy (3.07 GPa) increased to 3.43 GPa with 0.5 wt % MWCNT and 3.58 GPa with 0.7 wt % MXene. The highest flexural modulus for epoxy nanocomposites, reaching 3.93 GPa, was achieved

https://doi.org/10.1021/acsanm.3c05728
ACS Appl. Nano Mater. 2024, 7, 3314−3325

with 1 wt % MWCNT/MXene hybrid fillers, marking a remarkable 28% enhancement compared to neat epoxy. The trend in flexural strength within the nanocomposites paralleled that of the flexural modulus. Incorporating 0.5 wt % MWCNT and MXene led to improvements, increasing the flexural strength of neat epoxy (105.70 MPa) to 112.34 and 114.20 MPa, respectively. The highest flexural strength observed was 124.36 MPa with 1 wt % MWCNT/MXene hybrid fillers. The reinforcing mechanism is similar with the case of tensile test as discussed in Section 3.3.1.[48]

3.3.3. Toughness. Fracture toughness assessment of epoxy and its nanocomposites at different filler loadings was conducted through the SENB test, with the typical load–displacement curves presented in Figure 5a. Notably, all of the nanocomposite samples exhibited fracture at higher loads compared to neat epoxy. The enhancement in fracture toughness exhibited moderate improvement following the addition of 0.5 wt % MWCNT and MXene, with the most substantial improvement occurring with the incorporation of 1 wt % MWCNT/MXene hybrid fillers. Figure 5b illustrates the variation in fracture toughness with different filler loadings. The values are summarized in Table S3 in the Supporting Information. The fracture toughness of the neat epoxy measured 0.97 ± 0.04 MPa·m$^{1/2}$. With the addition of 0.5 wt % MWCNT and MXene, the fracture toughness improved to 1.44 ± 0.04 and 1.48 ± 0.02 MPa·m$^{1/2}$, respectively. However, the fracture properties experienced a decline beyond 0.5 wt % filler loading, likely due to the potential agglomeration of nanofillers within the epoxy matrix. In contrast, for MWCNT/MXene hybrid-reinforced nanocomposites, the fracture toughness continued to increase up to 1 wt % filler loading. With the addition of 1 wt % MWCNT/MXene hybrid, the fracture toughness reached an impressive value of 1.79 ± 0.06 MPa·m$^{1/2}$.

The fracture morphologies of epoxy composites reinforced with MWCNT and MXenes are shown in Figure 6. Red arrows in Figure 6a indicate the exposed MWCNTs and the imprints left behind following MWCNT pull-out. The primary energy dissipation mechanisms in play involve the debonding and pull-out of MWCNTs. When a crack opens, energy is dissipated by the frictional pull-out of MWCNTs from the epoxy matrix, which slows crack propagation (Figure 6d). For MXene-reinforced epoxy composites, crack deflection emerges as the key toughening mechanism, as depicted in Figure 6b. When the crack interacts with MXene, its trajectory shifts, leading to an increase in the fracture surface area. Consequently, this contributes to a higher fracture energy and enhanced fracture properties (Figure 6e). For the hybrid epoxy composite, both the pull-out of MWCNTs and crack deflection of MXenes contribute to higher fracture energy, as shown in Figure 6c,6f.

3.4. Electrical Properties. In Figure 7, the electrical conductivity of epoxy nanocomposites as a function of the filler weight percentage is shown. It can be realized that a conductive network was not constructed for MXene/epoxy nanocomposites. This phenomenon can be attributed to the rigid 2D structure of MXene, which is less prone to percolative network formation at low filler loadings (less than 1 wt % or 0.13 vol %), as depicted in Figure S5a. Generally, the percolation threshold for 2D nanofillers reinforced epoxy composites is higher than 2 wt %.[56] It should be noted that low percolation threshold (less than 1 wt %) has also been achieved for MXene-reinforced epoxy composites, induced due

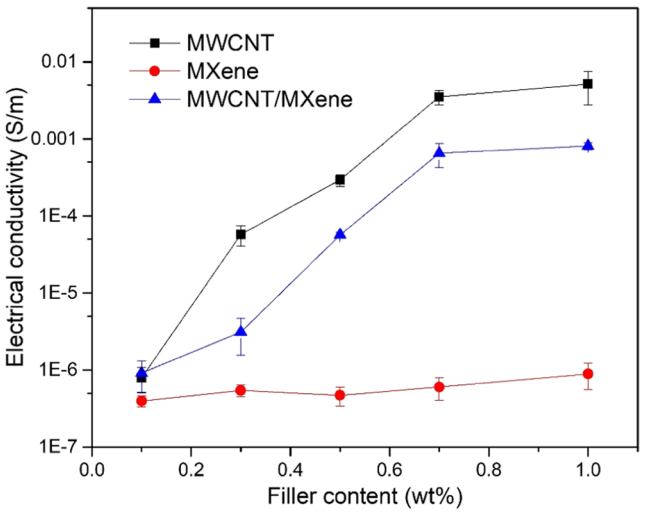

Figure 7. Variation of electrical conductivity of epoxy nanocomposites reinforced with MWCNT, MXene, and MWCNT/MXene hybrid.

to the presence of ultrathin MXene nanosheets.[22] In contrast, the epoxy nanocomposites reinforced by MWCNT were much more conductive than those reinforced by MXene. Compared to 2D MXene, 1D MWCNTs have higher aspect ratio, while their 1D nature contributes considerably more toward percolation, as shown in Figure S5b. These features facilitated the formation of multiple conductive paths within the matrix. The electrical conductivity of epoxy was improved to 2.95 × 10^{-4} S/m with 0.5 wt % MWCNT and 5.16 × 10^{-3} S/m with 1 wt % MWCNT, respectively. When MWCNT and MXenes were combined in the hybrid nanocomposites, the electrical conductivity was higher than the case of MXene and lower than the case of MWCNT. The MWCNTs bridged the broad conductivity gap between individual MXene nanosheets and MXene separated entangled MWCNTs from each other due to interfacial interactions, favoring the formation of a conductive path (Figure S5c). Therefore, the electrical conductivity was largely improved compared to the case of pure MXene nanocomposites. The electrical conductivity was improved to 5.71 × 10^{-5} S/m with 0.5 wt % MWCNT/MXene and 8.13 × 10^{-4} S/m with 1 wt % MWCNT/MXene, respectively. These values are about 1 order of magnitude lower than the values of MWCNT/epoxy nanocomposites. This can be attributed to the fact that a lower amount of MWCNTs was present in the hybrid composites compared to MWCNT/epoxy composites. As MWCNTs are more effective in constructing conductive paths due to their 1D structure and high aspect ratio, less conductive paths were constructed for the case of hybrid composites (Figure S5c).

3.5. Piezoresistive Properties. The addition of MWCNT and MWCNT/MXene hybrid allowed the epoxy matrix to display measurable conductivity. These levels of conductivity enable the utilization of the piezoresistive effect for monitoring the mechanical deformation of the nanocomposites. Subsequently, we explored the self-sensing capabilities of these nanocomposites during tensile, flexural, and fracture tests. For tensile and flexural tests, the change in the normalized resistance with applied strain was monitored. For fracture tests, the change in normalized resistance with displacement was monitored. Epoxy nanocomposites reinforced with 0.5 wt

https://doi.org/10.1021/acsanm.3c05728
ACS Appl. Nano Mater. 2024, 7, 3314–3325

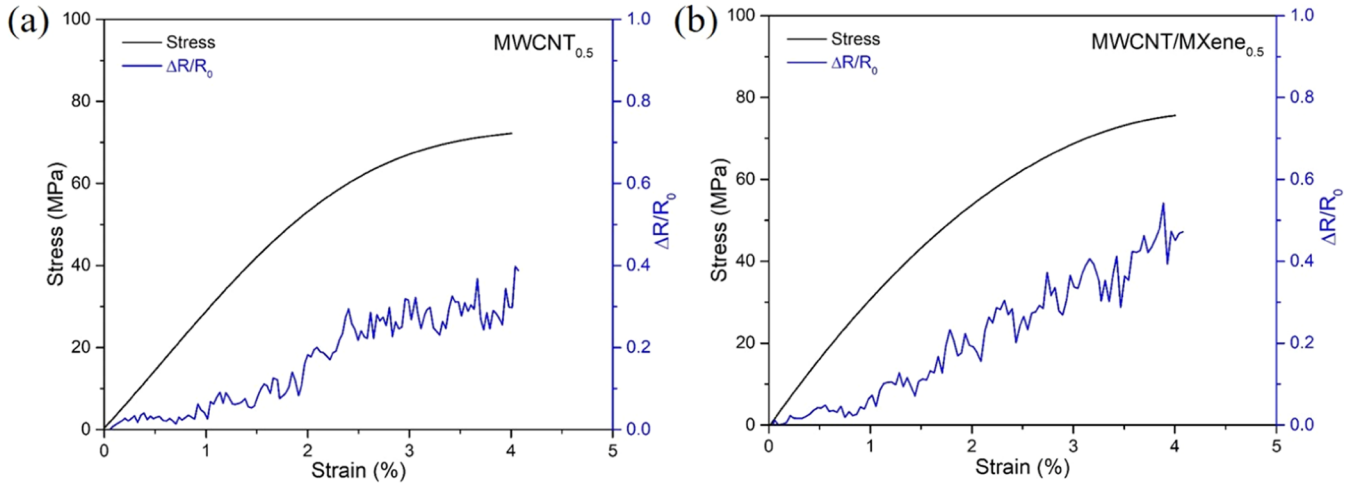

Figure 8. Piezoresistive response of the nanocomposites under tension (a) 0.5 wt % MWCNT/epoxy and (b) 0.5 wt % MWCNT/MXene epoxy nanocomposites.

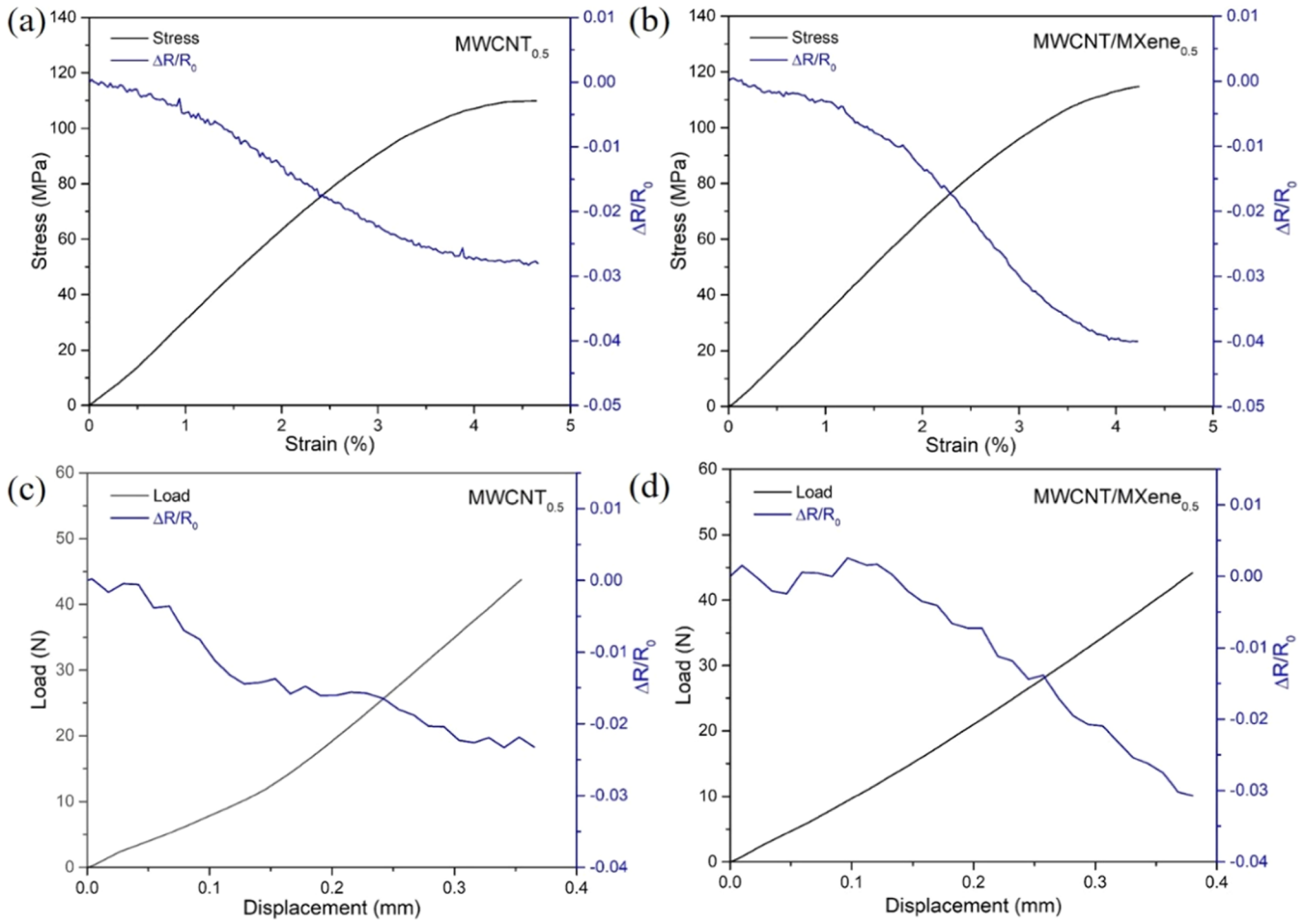

Figure 9. Piezoresistive response of the nanocomposites under flexural test: (a) 0.5 wt % MWCNT/epoxy and (b) 0.5 wt % MWCNT/MXene epoxy nanocomposites. Piezoresistive response of the nanocomposites under fracture test: (c) 0.5 wt % MWCNT/epoxy and (d) 0.5 wt % MWCNT/MXene epoxy nanocomposites.

% MWCNT and 0.5 wt % MWCNT/MXene hybrid were studied and compared.

3.5.1. Tensile Test. Figure 8a,b depicts the changes in electrical resistance concerning the applied tensile strain for epoxy nanocomposites containing 0.5 wt % MWCNT and 0.5 wt % MWCNT/MXene, respectively. In both cases, an increase in normalized resistance ($\Delta R/R_0$, where ΔR represents the change in electrical resistance and R_0 is the initial electrical resistance) was observed as the applied strain increased. This phenomenon can be attributed to the disruption of the conductive network within the matrix caused by the stretching of the composites.[57] As the applied strain

https://doi.org/10.1021/acsanm.3c05728
ACS Appl. Nano Mater. 2024, 7, 3314−3325

increased, the distance between neighboring fillers also increased, resulting in a decrease in the electrical pathways contributing to the piezoresistive behavior of the system.

As can be seen in Figure 8a,8b, the epoxy nanocomposite containing 0.5 wt % MWCNT/MXene hybrid exhibited greater sensitivity to tensile deformation when compared to its counterpart with 0.5 wt % MWCNT. For instance, at 3% applied strain, the increase in normalized resistance was 27% for the 0.5 wt % MWCNT/epoxy nanocomposite and 34% for the 0.5 wt % MWCNT/MXene/epoxy nanocomposite, highlighting the enhanced response of the latter. The sensitivity, known as gauge factor, can be calculated by the ratio of normalized resistance to strain as[58]

$$\mathrm{GF} = \frac{\Delta R/R_0}{\varepsilon} \tag{3}$$

where GF is the gauge factor and ε is the applied strain. Though there was no linear tendency, the gauge factor was calculated from the strain range from 0 to 1.5% to obtain a direct comparison. This discrepancy can be attributed to the fact that the epoxy nanocomposite containing 0.5 wt % MWCNT/MXene hybrid possesses fewer contact conductive pathways within the matrix, resulting in lower electrical conductivity (as shown in Figure 7). Consequently, when subjected to tensile deformation, it becomes more sensitive to the disruption of electrical contacts between particles.[59]

3.5.2. Flexural and Fracture Tests. Figure 9a,9b illustrates the electrical resistance responses of epoxy nanocomposites containing 0.5 wt % MWCNT and 0.5 wt % MWCNT/MXene. In both cases, the electrical resistance decreased as the applied strain increased. This phenomenon occurs because the distance between neighboring particles decreases on side of the sample that is under compression.[44] Once again, the epoxy nanocomposite featuring 0.5 wt % MWCNT/MXene hybrid demonstrated greater sensitivity compared to its 0.5 wt % MWCNT counterpart. At a 4% applied strain, the changes in normalized resistance were 2.7 and 4.0% for the 0.5 wt % MWCNT and 0.5 wt % MWCNT/MXene hybrid, respectively. It is worth noting that the changes in normalized resistance are considerably lower than those observed during tensile deformation. This can be attributed to the concurrent creation (in the compression side) and breakage (in the tension side) of electrically conductive pathways.[56]

The normalized resistance changes observed during fracture tests are depicted in Figure 9c,9d. In the SENB specimen, there was localized strain magnification at the notch, with stress combining both tension and compression globally throughout the specimen. As displacement increased, there was a downward trend in the normalized resistance, indicating that the dominant factor in the piezoresistive effect was the compressive strain. Notably, the hybrid nanocomposite exhibited a more substantial increase in the normalized resistance. At a 0.35 mm displacement, the change in normalized resistance was 2.2% for 0.5 wt % MWCNT and 2.8% for 0.5 wt % MWCNT/MXene hybrid, respectively. Furthermore, it is important to note that the sensitivity of the SENB specimen was lower than that of the tensile specimen, primarily due to the lower magnitude of strain and the localized nature of stress.[60]

4. CONCLUSIONS

In this study, two-phase (MWCNT/epoxy and MXene/epoxy) and three-phase (MWCNT/MXene/epoxy) nanocomposites were prepared by three-roll milling. The effects of MWCNT, MXene, and MWCNT/MXene hybrid on the mechanical, electrical, and piezoresistive properties of epoxy composites were studied in detail. Comparatively higher mechanical properties were observed in the three-phase composites when contrasted with their two-phase counterparts. Specifically, the incorporation of 1 wt % MWCNT/MXene hybrid led to substantial improvements in various properties of neat epoxy; the Young's modulus increased from 3.00 to 3.94 GPa, the flexural modulus rose from 3.07 to 3.93 GPa, and the fracture toughness improved from 0.97 to 1.79 MPa·m$^{1/2}$. This remarkable enhancement was supported by scanning electron microscopy images, which illustrated the prevention of individual filler aggregation in MWCNT/MXene hybrid-reinforced epoxy nanocomposites. Moreover, the three-phase composites exhibited heightened piezoresistive sensitivity in response to mechanical deformations, including tension, bending, and fracture. This enhanced sensitivity was attributed to the presence of a lower number of conductive contacts within the composite system.

The produced hybrid nanocomposites offer superior mechanical properties, electrical conductivity, and piezoresistive sensitivity. Their ability to enhance structural performance while simultaneously offering the real-time detection of deformations indicates promising applications in strain sensing and structural health monitoring. In addition, the hybrid composites also open up possibilities for a wide range of fields, such as E-heating and deicing applications.

■ ASSOCIATED CONTENT

Data Availability Statement

The raw data required to reproduce these findings are available on request.

Supporting Information

The Supporting Information is available free of charge at https://pubs.acs.org/doi/10.1021/acsanm.3c05728.

SEM of MAX, FTIR of fillers and epoxy composites, the codispersion mechanism, XRD of epoxy composites, tensile properties, flexural properties, and fracture toughness of epoxy composites, the rule of mixtures, and filler network (PDF)

■ AUTHOR INFORMATION

Corresponding Authors

Ming Dong − *School of Physical and Chemical Sciences, Queen Mary University of London, London E1 4NS, U.K.;* orcid.org/0000-0002-4070-100X; Email: m.dong@qmul.ac.uk

Dimitrios G. Papageorgiou − *School of Engineering and Materials Science, Queen Mary University of London, London E1 4NS, U.K.;* orcid.org/0000-0001-5558-5040; Email: d.papageorgiou@qmul.ac.uk

Authors

Oliver Tomes − *School of Engineering and Materials Science, Queen Mary University of London, London E1 4NS, U.K.;* orcid.org/0009-0006-4492-2754

Aaron Soul − *School of Engineering and Materials Science, Queen Mary University of London, London E1 4NS, U.K.*

Yi Hu − *School of Engineering and Materials Science, Queen Mary University of London, London E1 4NS, U.K.*

Emiliano Bilotti − *Department of Aeronautics, Imperial College London, London SW7 2AZ, U.K.;* orcid.org/0000-0003-3952-1148

Han Zhang − *School of Engineering and Materials Science, Queen Mary University of London, London E1 4NS, U.K.;* orcid.org/0000-0002-0479-224X

Complete contact information is available at: https://pubs.acs.org/10.1021/acsanm.3c05728

Notes

The authors declare no competing financial interest.

REFERENCES

(1) Jin, F. L.; Li, X.; Park, S. J. Synthesis and application of epoxy resins: A review. *J. Ind. Eng. Chem.* **2015**, *29*, 1−11.

(2) Ahmadi, Z. Epoxy in nanotechnology: A short review. *Prog. Org. Coat.* **2019**, *132*, 445−448.

(3) Gu, H.; Ma, C.; Gu, J.; Guo, J.; Yan, X.; Huang, J.; Zhang, Q.; Guo, Z. An overview of multifunctional epoxy nanocomposites. *J. Mater. Chem. C* **2016**, *4* (25), 5890−5906.

(4) Dong, M.; Zhang, H.; Tzounis, L.; Santagiuliana, G.; Bilotti, E.; Papageorgiou, D. G. Multifunctional epoxy nanocomposites reinforced by two-dimensional materials: A review. *Carbon* **2021**, *185*, 57−81.

(5) Liang, C.; Song, P.; Gu, H.; Ma, C.; Guo, Y.; Zhang, H.; Xu, X.; Zhang, Q.; Gu, J. Nanopolydopamine coupled fluorescent nanozinc oxide reinforced epoxy nanocomposites. *Composites, Part A* **2017**, *102*, 126−136.

(6) Singh, N. P.; Gupta, V. K.; Singh, A. P. Graphene and carbon nanotube reinforced epoxy nanocomposites: A review. *Polymer* **2019**, *180*, No. 121724.

(7) Papageorgiou, D. G.; Li, Z. L.; Liu, M. F.; Kinloch, I. A.; Young, R. J. Mechanisms of mechanical reinforcement by graphene and carbon nanotubes in polymer nanocomposites. *Nanoscale* **2020**, *12* (4), 2228−2267.

(8) Tang, L.-C.; Wan, Y.-J.; Peng, K.; Pei, Y.-B.; Wu, L.-B.; Chen, L.-M.; Shu, L.-J.; Jiang, J.-X.; Lai, G.-Q. Fracture toughness and electrical conductivity of epoxy composites filled with carbon nanotubes and spherical particles. *Composites, Part A* **2013**, *45*, 95−101.

(9) De Volder, M. F. L.; Tawfick, S. H.; Baughman, R. H.; Hart, A. J. Carbon Nanotubes: Present and Future Commercial Applications. *Science* **2013**, *339* (6119), 535−539.

(10) Ajayan, P. M.; Schadler, L. S.; Giannaris, C.; Rubio, A. Single-Walled Carbon Nanotube−Polymer Composites: Strength and Weakness. *Adv. Mater.* **2000**, *12* (10), 750−753.

(11) Sandler, J. K. W.; Kirk, J. E.; Kinloch, I. A.; Shaffer, M. S. P.; Windle, A. H. Ultra-low electrical percolation threshold in carbon-nanotube-epoxy composites. *Polymer* **2003**, *44* (19), 5893−5899.

(12) Rafiee, M. A.; Rafiee, J.; Wang, Z.; Song, H.; Yu, Z.-Z.; Koratkar, N. Enhanced Mechanical Properties of Nanocomposites at Low Graphene Content. *ACS Nano* **2009**, *3* (12), 3884−3890.

(13) Cha, J.; Kim, J.; Ryu, S.; Hong, S. H. Comparison to mechanical properties of epoxy nanocomposites reinforced by functionalized carbon nanotubes and graphene nanoplatelets. *Composites, Part B* **2019**, *162*, 283−288.

(14) Naguib, M.; Kurtoglu, M.; Presser, V.; Lu, J.; Niu, J. J.; Heon, M.; Hultman, L.; Gogotsi, Y.; Barsoum, M. W. Two-Dimensional Nanocrystals Produced by Exfoliation of Ti_3AlC_2. *Adv. Mater.* **2011**, *23* (37), 4248−4253.

(15) Lipatov, A.; Lu, H. D.; Alhabeb, M.; Anasori, B.; Gruverman, A.; Gogotsi, Y.; Sinitskii, A. Elastic properties of 2D $Ti_3C_2T_x$ MXene monolayers and bilayers. *Sci. Adv.* **2018**, *4* (6), No. eaat0491.

(16) Lipatov, A.; Goad, A.; Loes, M. J.; Vorobeva, N. S.; Abourahma, J.; Gogotsi, Y.; Sinitskii, A. High electrical conductivity and breakdown current density of individual monolayer $Ti_3C_2T_x$ MXene flakes. *Matter* **2021**, *4* (4), 1413−1427.

(17) Dong, M.; Hu, Y.; Zhang, H.; Bilotti, E.; Pugno, N.; Dunstan, D.; Papageorgiou, D. G. Micromechanics of $Ti_3C_2T_x$ MXene reinforced poly(vinyl alcohol) nanocomposites. *JCOMC* **2024**, *13*, No. 100427.

(18) Zhang, Y.; Ruan, K.; Guo, Y.; Gu, J. Recent Advances of MXenes-Based Optical Functional Materials. *Adv. Photonics* **2023**, *4* (12), No. 2300224.

(19) Zhang, Y.; Ruan, K.; Zhou, K.; Gu, J. Controlled Distributed $Ti_3C_2T_x$ Hollow Microspheres on Thermally Conductive Polyimide Composite Films for Excellent Electromagnetic Interference Shielding. *Adv. Mater.* **2023**, *35* (16), No. 2211642.

(20) Song, P.; Liu, B.; Qiu, H.; Shi, X.; Cao, D.; Gu, J. MXenes for polymer matrix electromagnetic interference shielding composites: A review. *Compos. Commun.* **2021**, *24*, No. 100653.

(21) Giménez, R.; Serrano, B.; San-Miguel, V.; Cabanelas, J. C. Recent Advances in MXene/Epoxy Composites: Trends and Prospects. *Polymers* **2022**, *14* (6), No. 1170.

(22) Wang, L.; Chen, L. X.; Song, P.; Liang, C. B.; Lu, Y. J.; Qiu, H.; Zhang, Y. L.; Kong, J.; Gu, J. W. Fabrication on the annealed $Ti_3C_2T_x$ MXene/Epoxy nanocomposites for electromagnetic interference shielding application. *Composites, Part B* **2019**, *171*, 111−118.

(23) Liu, L.; Ying, G.; Wen, D.; Zhang, K.; Hu, C.; Zheng, Y.; Zhang, C.; Wang, X.; Wang, C. Aqueous solution-processed MXene ($Ti_3C_2T_x$) for non-hydrophilic epoxy resin-based composites with enhanced mechanical and physical properties. *Mater. Des.* **2021**, *197*, No. 109276.

(24) Wazalwar, R.; Tripathi, M.; Raichur, A. M. Curing Behavior and Mechanical Properties of Tetra-Functional Epoxy Reinforced with Polyethyleneimine-Functionalized MXene. *ACS Appl. Polym. Mater.* **2022**, *4* (4), 2573−2584.

(25) Kang, R. Y.; Zhang, Z. Y.; Guo, L. C.; Cui, J. F.; Chen, Y. P.; Hou, X.; Wang, B.; Lin, C. T.; Jiang, N.; Yu, J. H. Enhanced Thermal Conductivity of Epoxy Composites Filled with 2D Transition Metal Carbides (MXenes) with Ultralow Loading. *Sci. Rep.* **2019**, *9*, No. 9135.

(26) Chen, L.; Cao, Y.; Zhang, X.; Guo, X.; Song, P.; Chen, K.; Lin, J. Anisotropic and high thermal conductivity of epoxy composites containing multilayer $Ti_3C_2T_x$ MXene nanoflakes. *J. Mater. Sci.* **2020**, *55* (35), 16533−16543.

(27) Feng, A. L.; Hou, T. Q.; Jia, Z. R.; Zhang, Y.; Zhang, F.; Wu, G. L. Preparation and Characterization of Epoxy Resin Filled with $Ti_3C_2T_x$ MXene Nanosheets with Excellent Electric Conductivity. *Nanomaterials* **2020**, *10* (1), No. 162.

(28) Yan, H. Y.; Tang, Y. X.; Su, J. L.; Yang, X. Y. Enhanced thermal-mechanical properties of polymer composites with hybrid boron nitride nanofillers. *Appl. Phys. A* **2014**, *114* (2), 331−337.

(29) Zhang, C.; Huang, S.; Tjiu, W. W.; Fan, W.; Liu, T. X. Facile preparation of water-dispersible graphene sheets stabilized by acid-treated multi-walled carbon nanotubes and their poly(vinyl alcohol) composites. *J. Mater. Chem.* **2012**, *22* (6), 2427−2434.

(30) Liu, L.; Ying, G.; Sun, C.; Min, H.; Zhang, J.; Zhao, Y.; Wen, D.; Ji, Z.; Liu, X.; Zhang, C.; Wang, C. MXene ($Ti_3C_2T_x$) Functionalized Short Carbon Fibers as a Cross-Scale Mechanical Reinforcement for Epoxy Composites. *Polymers* **2021**, *13* (11), No. 1825.

(31) Xu, X.; Chen, Y.; He, P.; Wang, S.; Ling, K.; Liu, L.; Lei, P.; Huang, X.; Zhao, H.; Cao, J.; Yang, J. Wearable CNT/$Ti_3C_2T_x$ MXene/PDMS composite strain sensor with enhanced stability for real-time human healthcare monitoring. *Nano Res.* **2021**, *14* (8), 2875−2883.

(32) Szeluga, U.; Kumanek, B.; Trzebicka, B. Synergy in hybrid polymer/nanocarbon composites. A review. *Composites, Part A* **2015**, *73*, 204−231.

(33) Yang, S. Y.; Lin, W. N.; Huang, Y. L.; Tien, H. W.; Wang, J. Y.; Ma, C. C. M.; Li, S. M.; Wang, Y. S. Synergetic effects of graphene platelets and carbon nanotubes on the mechanical and thermal properties of epoxy composites. *Carbon* **2011**, *49* (3), 793−803.

(34) Li, W.; Dichiara, A.; Bai, J. Carbon nanotube−graphene nanoplatelet hybrids as high-performance multifunctional reinforcements in epoxy composites. *Compos. Sci. Technol.* **2013**, *74*, 221−227.
(35) Yue, L.; Pircheraghi, G.; Monemian, S. A.; Manas-Zloczower, I. Epoxy composites with carbon nanotubes and graphene nanoplatelets − Dispersion and synergy effects. *Carbon* **2014**, *78*, 268−278.
(36) Im, H.; Kim, J. Thermal conductivity of a graphene oxide−carbon nanotube hybrid/epoxy composite. *Carbon* **2012**, *50* (15), 5429−5440.
(37) Wang, Y. F.; Liang, L. Y.; Du, Z. R.; Wang, Y. M.; Liu, C. T.; Shen, C. Y. Biodegradable PLA/CNTs/$Ti_3C_2T_x$ MXene nanocomposites for efficient electromagnetic interference shielding. *J. Mater. Sci.: Mater. Electron.* **2021**, *32* (21), 25952−25962.
(38) Aakyiir, M.; Oh, J. A.; Araby, S.; Zheng, Q. H.; Naeem, M.; Ma, J.; Adu, P.; Zhang, L. Q.; Mai, Y. W. Combining hydrophilic MXene nanosheets and hydrophobic carbon nanotubes for mechanically resilient and electrically conductive elastomer nanocomposites. *Compos. Sci. Technol.* **2021**, *214*, No. 108997.
(39) Jia, P.; Lu, J.; He, R.; Jiang, G.; Jiang, X.; Wang, B.; Song, L.; Hu, Y. Octopus sucker-inspired hierarchical structure MXene@carbon nanotubes enhancing the mechanical properties and fire safety of thermoplastic polyurethane composites through the interfacial engineering. *Chem. Eng. J.* **2022**, *450*, No. 138184.
(40) Alhabeb, M.; Maleski, K.; Anasori, B.; Lelyukh, P.; Clark, L.; Sin, S.; Gogotsi, Y. Guidelines for Synthesis and Processing of Two-Dimensional Titanium Carbide ($Ti_3C_2T_x$ MXene). *Chem. Mater.* **2017**, *29* (18), 7633−7644.
(41) Li, Y.; Zhang, H.; Crespo, M.; Porwal, H.; Picot, O.; Santagiuliana, G.; Huang, Z. H.; Barbieri, E.; Pugno, N. M.; Peijs, T.; Bilotti, E. In Situ Exfoliation of Graphene in Epoxy Resins: A Facile Strategy to Efficient and Large Scale Graphene Nanocomposites. *ACS Appl. Mater. Interfaces* **2016**, *8* (36), 24112−24122.
(42) Li, Y.; Zhang, H.; Porwal, H.; Huang, Z.; Bilotti, E.; Peijs, T. Mechanical, electrical and thermal properties of in-situ exfoliated graphene/epoxy nanocomposites. *Composites, Part A* **2017**, *95*, 229−236.
(43) Dong, M.; Hu, Y.; Yu, X.; Liu, M.; Bilotti, E.; Zhang, H.; Papageorgiou, D. G. Probing Interfacial Interactions in Ternary Nanocomposites of $Ti_3C_2T_x$ MXene Nanoplatelets, Multiwalled Carbon Nanotubes, and Poly(vinyl alcohol) toward Synergistic Reinforcement. *ACS Appl. Polym. Mater.* **2024**, *6*, 207−217.
(44) Kernin, A.; Wan, K.; Liu, Y.; Shi, X.; Kong, J.; Bilotti, E.; Peijs, T.; Zhang, H. The effect of graphene network formation on the electrical, mechanical, and multifunctional properties of graphene/epoxy nanocomposites. *Compos. Sci. Technol.* **2019**, *169*, 224−231.
(45) Chandrasekaran, S.; Sato, N.; Tölle, F.; Mülhaupt, R.; Fiedler, B.; Schulte, K. Fracture toughness and failure mechanism of graphene based epoxy composites. *Compos. Sci. Technol.* **2014**, *97*, 90−99.
(46) Hu, Y.; Pang, S.; Li, J.; Jiang, J.; Papageorgiou, D. G. Enhanced interfacial properties of hierarchical MXene/CF composites via low content electrophoretic deposition. *Composites, Part B* **2022**, *237*, No. 109871.
(47) Dresselhaus, M. S.; Dresselhaus, G.; Saito, R.; Jorio, A. Raman spectroscopy of carbon nanotubes. *Phys. Rep.* **2005**, *409* (2), 47−99.
(48) Zakaria, M. R.; Kudus, M. H. A.; Akil, H. M.; Thirmizir, M. Z. M. Comparative study of graphene nanoparticle and multiwall carbon nanotube filled epoxy nanocomposites based on mechanical, thermal and dielectric properties. *Composites, Part B* **2017**, *119*, 57−66.
(49) Sarycheva, A.; Gogotsi, Y. Raman Spectroscopy Analysis of the Structure and Surface Chemistry of $Ti_3C_2T_x$ MXene. *Chem. Mater.* **2020**, *32* (8), 3480−3488.
(50) Avilés, F.; Cauich-Rodríguez, J. V.; Moo-Tah, L.; May-Pat, A.; Vargas-Coronado, R. Evaluation of mild acid oxidation treatments for MWCNT functionalization. *Carbon* **2009**, *47* (13), 2970−2975.
(51) Kiran, N. U.; Deore, A. B.; More, M. A.; Late, D. J.; Rout, C. S.; Mane, P.; Chakraborty, B.; Besra, L.; Chatterjee, S. Comparative Study of Cold Electron Emission from 2D $Ti_3C_2T_x$ MXene Nanosheets with Respect to Its Precursor Ti_3SiC_2 MAX Phase. *ACS Appl. Electron. Mater.* **2022**, *4* (6), 2656−2666.
(52) Ramezanzadeh, M.; Ramezanzadeh, B. Covalent Organic Framework (COF)-decorated NH_2-functionalized MXene sheets for Thermomechanical and UV-Shielding Performance of Epoxy Nanocomposite Coatings. *Colloids Surf., A* **2023**, *683*, No. 133010.
(53) Dong, M.; Young, R. J.; Dunstan, D. J.; Papageorgiou, D. G. Interfacial stress transfer in monolayer and few-layer MoS_2 nanosheets in model nanocomposites. *Compos. Sci. Technol.* **2023**, *233*, No. 109892.
(54) Young, R. J.; Liu, M. F.; Kinloch, I. A.; Li, S. H.; Zhao, X.; Valles, C.; Papageorgiou, D. G. The mechanics of reinforcement of polymers by graphene nanoplatelets. *Compos. Sci. Technol.* **2018**, *154*, 110−116.
(55) Papageorgiou, D. G.; Kinloch, I. A.; Young, R. J. Hybrid multifunctional graphene/glass-fibre polypropylene composites. *Compos. Sci. Technol.* **2016**, *137*, 44−51.
(56) Moriche, R.; Sánchez, M.; Jiménez-Suárez, A.; Prolongo, S. G.; Ureña, A. Strain monitoring mechanisms of sensors based on the addition of graphene nanoplatelets into an epoxy matrix. *Compos. Sci. Technol.* **2016**, *123*, 65−70.
(57) Sanli, A.; Müller, C.; Kanoun, O.; Elibol, C.; Wagner, M. F. X. Piezoresistive characterization of multi-walled carbon nanotube-epoxy based flexible strain sensitive films by impedance spectroscopy. *Compos. Sci. Technol.* **2016**, *122*, 18−26.
(58) Biccai, S.; Boland, C. S.; O'Driscoll, D. P.; Harvey, A.; Gabbett, C.; O'Suilleabhain, D. R.; Griffin, A. J.; Li, Z.; Young, R. J.; Coleman, J. N. Negative Gauge Factor Piezoresistive Composites Based on Polymers Filled with MoS_2 Nanosheets. *ACS Nano* **2019**, *13* (6), 6845−6855.
(59) Ke, K.; Solouki Bonab, V.; Yuan, D.; Manas-Zloczower, I. Piezoresistive thermoplastic polyurethane nanocomposites with carbon nanostructures. *Carbon* **2018**, *139*, 52−58.
(60) Esmaeili, A.; Sbarufatti, C.; Jiménez-Suárez, A.; Hamouda, A. M. S.; Rovatti, L.; Ureña, A. Synergistic effects of double-walled carbon nanotubes and nanoclays on mechanical, electrical and piezoresistive properties of epoxy based nanocomposites. *Compos. Sci. Technol.* **2020**, *200*, No. 108459.

https://doi.org/10.1021/acsanm.3c05728
ACS Appl. Nano Mater. 2024, 7, 3314−3325